Journal of Solid State Chemistry **156,** 194–202 (2001)
doi:10.1006/jssc.2000.8981, available online at http://www.idealibrary.com on IDEAL®

Determination of the Oxidation States of Cu and Ru in the System $La_{2-x}Sr_xCu_{1-y}Ru_yO_{4-\delta}$ by XANES-Measurements

Stefan Ebbinghaus,*,[1] Zhiwei Hu,† and Armin Reller*

*Institut für Physik, Universität Augsburg, Universitätsstrasse 1, D-86159 Augsburg, Germany; and †Institut für Festkörper- und Werkstofforschung Dresden, D-01171 Dresden, Germany

Received June 14, 2000; in revised form August 23, 2000; accepted October 3, 2000; published online December 21, 2000

Numerous samples of the system $La_{2-x}Sr_xCu_{1-y}Ru_yO_{4-\delta}$ ($0.86 \leq x \leq 2$, $0.05 \leq y \leq 1$) as well as several other cuprates and ruthenates have been investigated by XANES spectroscopy. The exact energy positions of the white lines observed at the Cu– and Ru–L_{III} absorption edges are a sensitive measure for the oxidation state of the corresponding transition metal. Our results lead to the following fundamental conclusions: (i) Charge compensation in the system $La_{2-x}Sr_xCu_{1-y}Ru_yO_{4-\delta}$ is achieved by a successive oxidation of Ru^{4+} to Ru^{5+}, while copper remains in the oxidation state 2+. (ii) The formation of Ru^{6+} ions or higher oxidized species can be ruled out. (iii) For those compounds in which charge neutrality is not possible by the formation of Ru^{5+} alone, the remaining electron "holes" are located at the oxygen sites. The possibility of using the valence shift as a quantitative measure for the oxidation state of Ru in new compounds is briefly discussed.

Key Words: **XANES; oxidation states; perovskites; cuprates; ruthenates.**

INTRODUCTION

One of the key problems in metal oxide chemistry is the accurate determination of oxidation states. Imagine, for example, a perovskite-related material with the general composition $AB_{1-y}B'_yO_{3-\delta}$ in which both elements B and B′ are able to adopt two different oxidation states (say $+n$ and $+(n-1)$): The determination of the total oxygen content $(3-\delta)$ will lead only to an average oxidation number of the B-type cations but does not provide any element-specific information. So the question which of the cations (B or B′) becomes oxidized (or reduced) by changing δ remains unsolved. This situation becomes even worse if B and B′ can obey more than two different oxidation states or if the perovskite contains more than two redox-active elements. In special cases it might be possible to selectively reduce one element either by titration or by thermogravimetric reduction in a suitable atmosphere. Nevertheless, a more general approach would highly be desirable.

In recent years X-ray absorption spectroscopy (XAS) has been applied as an extremely useful tool for determining the oxidation state of transition metal ions. For a given metal the energies of the absorption edges increase with increasing charge. The origin for this so-called "valence shift" is the fact that the positive electric charge of the nucleus is partially shielded by the *d* electrons. If, by oxidation of the metal, the number of valence electrons is reduced, the effective core charge increases and the inner electrons become more tightly bound. As a result, more energy is required for the promotion of such an electron and its absorption edge is shifted towards higher energy values. Some nice examples for the valence shift effect in Ir-, Os-, and Ru-containing perovskites can be found in references (1–4).

In this article we report the determination of the oxidation states of Cu and Ru in the perovskite-related system $La_{2-x}Sr_xCu_{1-y}Ru_yO_{4-\delta}$ by XANES (X-ray absorption near edge structure) spectroscopy. Thermogravimetric measurements of the oxygen content had revealed that for $x > 2y$ parts of the B-type cations must possess an increased oxidation state (5). In principal, both Cu and Ru may become higher oxidized. In a previous article the examination of the local Cu and Ru environments by EXAFS (extended X-ray absorption fine structure) spectroscopy was reported (6). One of the major results was that the oxygen vacancies are exclusively located in the copper surrounding while ruthenium remains in an octahedral coordination sphere. This finding already indicated that Ru rather than Cu would become oxidized. The results presented in this paper turned out to be an excellent verification of this assumption.

XANES measurements were performed at the metal–L_{III} edges as these show very intense "white lines" which result from inner-atomic transitions of the $2p$ core electrons to unoccupied bound states with predominantly *d* character ($l = 2$). These transitions therefore can be used as a probe to examine the valence orbitals. Because of the $\Delta l = \pm 1$

[1] To whom correspondence should be addressed. Fax: ++49 821 598 3002. E-mail: stefan.ebbinghaus@physik.uni-augsburg.de.

0022-4596/01 $35.00

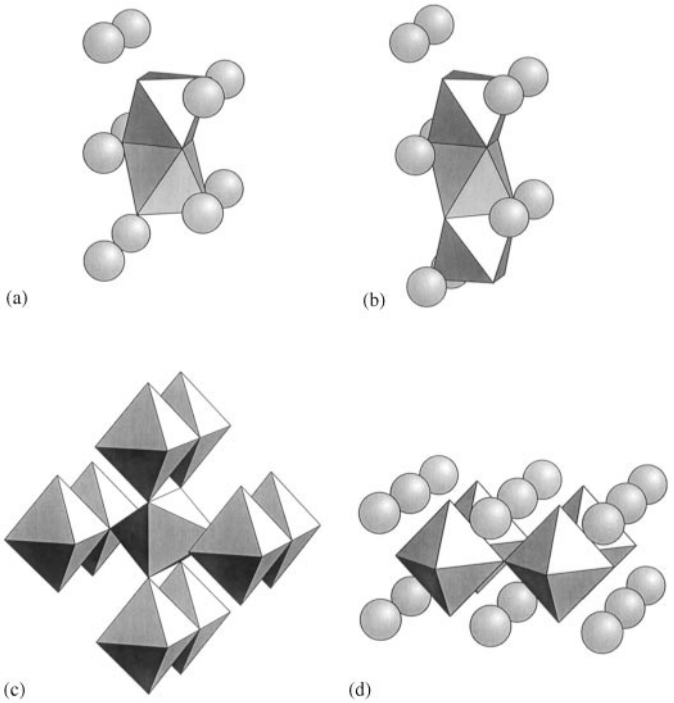

FIG. 1. Local environment of Ru in $Sr_4Ru_2O_9$ and $Ba_5Ru_2O_9(O_2)$ (a), $Ba_5Ru_3O_{12}$ (b), RuO_2 (c) and $La_{2-x}Sr_xCu_{1-y}Ru_yO_{4-\delta}$ (d). The octahedra represent the RuO_6 units while the spheres are the A-type cations (Sr, Ba, and La).

selection rule for dipole transitions no white lines are observed at the K and the L_I edge which both start from s-type ground states ($l = 0$).

For an accurate determination of oxidation states it is essential to examine reference materials. Therefore, we also report the XANES results for several other copper and ruthenium oxides: In the case of copper, CuO and $La_2Li_{0.5}Cu_{0.5}O_4$ were used as Cu^{2+} and Cu^{3+} standards. For ruthenium, we have measured Sr_2RuO_4 and RuO_2 as Ru^{4+} standards while $Ba_5Ru_2O_9(O_2)$ and $Sr_4Ru_2O_9$ served as Ru^{5+} references. The mixed valence oxide $Ba_5Ru_3O_{12}$ ($Ru^{4.67+}$) was also investigated. In all compounds ruthenium possesses an (slightly distorted) octahedral oxygen coordination comparable to the one in $La_{2-x}Sr_xCu_{1-y}Ru_yO_{4-\delta}$. This is important because the absorption edge fine structure of a specific element is strongly influenced by the nature of its ligands (e.g., because of the degree of covalence in the bonding) giving rise to the so-called "chemical shift." Therefore, only compounds with similar chemical environment may be compared. The relevant parts of the different crystal structures are shown in Fig. 1.

EXPERIMENTAL

The preparation and characterization of compounds belonging to the $La_{2-x}Sr_xCu_{1-y}Ru_yO_{4-\delta}$ system, $Ba_5Ru_2O_9(O_2)$, $Sr_4Ru_2O_9$, and $Ba_5Ru_3O_{12}$ are described in Refs. (5), (7), (8), and (9), respectively. The commercially available RuO_2 (Fluka) was dried at 600°C prior to the measurements.

The Cu–L_{III} XAS data were recorded at the SX700/II beamline of the Berliner Elektronen Speicherring für Synchrotronstrahlung (BESSY) in fluorescence yield mode. For each measurement approximately 0.4 g oxide was pelletized and the sample was scraped in vacuum ($p = 5 \times 10^{-10}$ mbar) with a diamond file to obtain a clean surface. A stepwidth of 0.1 eV and a counting time of 1 s/data point were applied. CuO was used as standard for the energy calibration. XANES investigations at the Ru–L_{III} edge were carried out at the beamline E4 of the Hamburger Synchrotronstrahlungslabor (HASYLAB) at the Deutsches Elektronensynchrotron (DESY). Depending on the Ru content, about 5–10 mg of oxide was mixed with 20 mg polyethylene powder and pressed into a pellet of 13 mm diameter. The measurements were performed in transmission mode using a step width of 0.2 eV and a counting time of 2 s per data point. For energy calibration a small amount (20 Torr) of Ar was added to the absorption gas in the last ionization chamber, leading to a very intense and sharp peak at $E \approx 3.2$ keV. The maximum of this peak was assigned to the energy position of the Ar–K edge (3.2029 keV).

Data evaluation was carried out using the program WinXAS (10). After calibration of the energy scale a background correction was done by fitting the pre-edge region with a Victoreen-type function. This function was then extrapolated over the whole spectrum and subtracted from the data. The edge jump was normalized by setting the average absorption coefficient between 2.861 and 2.867 keV to the value *1*.

RESULTS AND DISCUSSION

Cu–L_{III} XANES

Figure 2 shows the absorption spectra of some selected samples in comparison with the references CuO and $La_2Li_{0.5}Cu_{0.5}O_4$ in which Cu obeys the formal oxidation states 2+ and 3+, respectively. As can clearly be seen, the absorption spectrum of CuO consists of one strong white line at 931.2 eV which arises from a transition $2p3d^9 \rightarrow \underline{2p}3d^{10}$ typical for Cu^{2+}. In contrast, the absorption peak of Cu^{3+} in $La_2Li_{0.5}Cu_{0.5}O_4$ is shifted by 1.7 eV toward higher energies. This peak was assigned to a transition leading to a final state with predominantly $\underline{2p}3d^{10}\underline{L}$ character ($\underline{L}$ describing an electron hole in the oxygen 2p orbitals) (11).

Looking at the spectra of the system $La_{2-x}Sr_xCu_{1-y}Ru_yO_{4-\delta}$ it is evident that all samples exhibit the same absorption features as the Cu^{2+} standard. The differences in the exact peak position with respect to CuO were

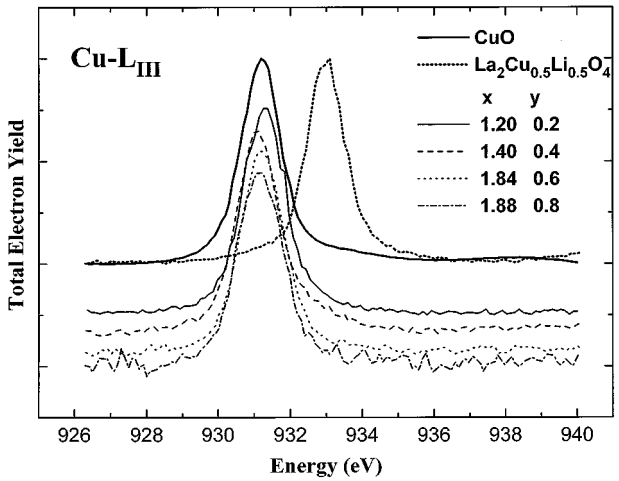

FIG. 2. Normalized Cu–L_{III} XANES spectra of selected samples of the system $La_{2-x}Sr_xCu_{1-y}Ru_yO_{4-\delta}$ in comparison to the Cu^{2+} and Cu^{3+} reference materials.

typically in the order of ± 0.2 eV. No systematic relationship between these small energy shifts and the composition could be detected. We therefore conclude that copper remains in the oxidation state $2+$ in all samples, while the formation of Cu^{3+} can be ruled out.

For the two samples $La_{1.14}Sr_{0.86}Cu_{0.95}Ru_{0.05}O_{4-\delta}$ and $La_{0.64}Sr_{1.36}Cu_{0.8}Ru_{0.2}O_{4-\delta}$ a weak shoulder at higher energies was observed. This shoulder has already been detected in cuprate superconductors like $YBa_2Cu_3O_{7-\delta}$ (12, 13) and is supposed to belong to a $3d^9\underline{L}$ ground state (14, 15). Therefore, the intensity of this shoulder is a measure of the density of holes in the oxygen $2p$ orbitals. The fact that we observed this shoulder only for very high ratios $x/2y$ and high copper concentrations indicates that the $3d^9\underline{L}$ configuration occurs only when other routes to achieve charge balance (like the formation of Ru^{5+}—see below—or an increase of the oxygen deficit δ) are exhausted. Figure 3 shows the Cu–L_{III} spectra of the two compounds and the well-known superconductor (La, Sr)CuO_4 in comparison with CuO, which has a pure $3d^9$ ground state. Although the described shoulder seems to be typical for cuprate superconductors, both samples turned out to be non-superconducting (16).

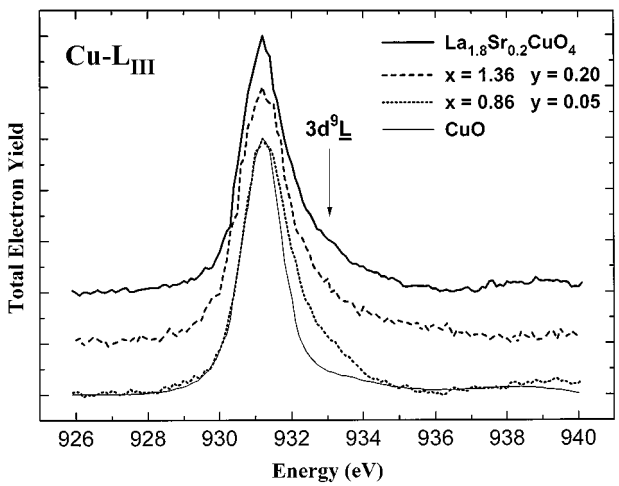

FIG. 3. The $3d^9\underline{L}$ related shoulder in the Cu–L_{III} XANES spectra of the two compounds with the highest ratios $x/2y$ in comparison to $La_{1.8}Sr_{0.2}CuO_4$ and CuO.

Ru–L_{III} XANES

In contrast to the Cu–L XANES, the Ru–L_{III} absorption spectra of the various samples showed pronounced differences. In Fig. 4 the spectra of some selected compounds are depicted. For the sake of clearness the peak heights have been normalized. It can easily be seen that, going from Sr_2RuO_4 to $La_{0.84}Sr_{1.16}Cu_{0.7}Ru_{0.3}O_{4-\delta}$, the white line splits into two well separated peaks and shifts toward higher energies. The fact that two peaks are found at the Ru–L_{III} threshold is due to the splitting of the Ru d orbitals into sets of t_{2g}- and e_g-symmetry by the cubic crystal field. For Cu^{2+} with its d^9 configuration, only the transition to the half unoccupied e_g orbital ($d_x^2 - d_y^2$) is possible, and therefore only one white line is observed. For Ru^{4+} ($4d^4$) and higher oxidized species, on the other hand, both transitions to the t_{2g} and e_g orbitals occur, leading to two distinct white lines. A closer examination reveals that both sets of orbitals are further split due to the spin-orbit coupling and a possible tetragonal distortion of the crystal field (17). Nevertheless, as these splittings are small compared to 10Dq it is a reasonable approximation to assign the two peaks to transitions to the t_{2g} and e_g orbitals, respectively.

Thermogravimetric measurements described in Ref. (5) revealed that in the system $La_{2-x}Sr_xCu_{1-y}Ru_yO_{4-\delta}$ the

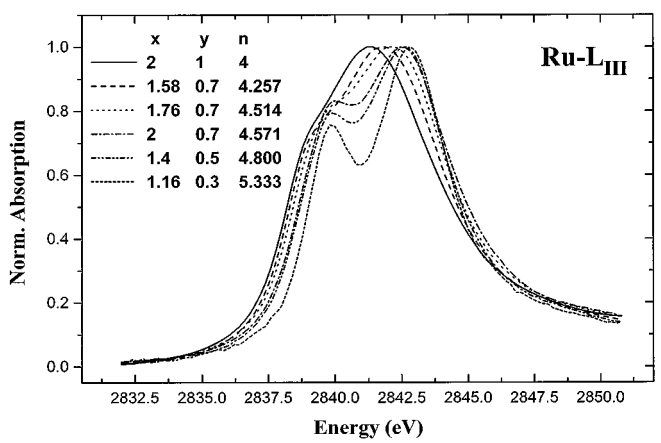

FIG. 4. Normalized Ru-L_{III} XANES spectra of selected samples of the system $La_{2-x}Sr_xCu_{1-y}Ru_yO_{4-\delta}$. n denotes the average oxidation state according to Eq. [2].

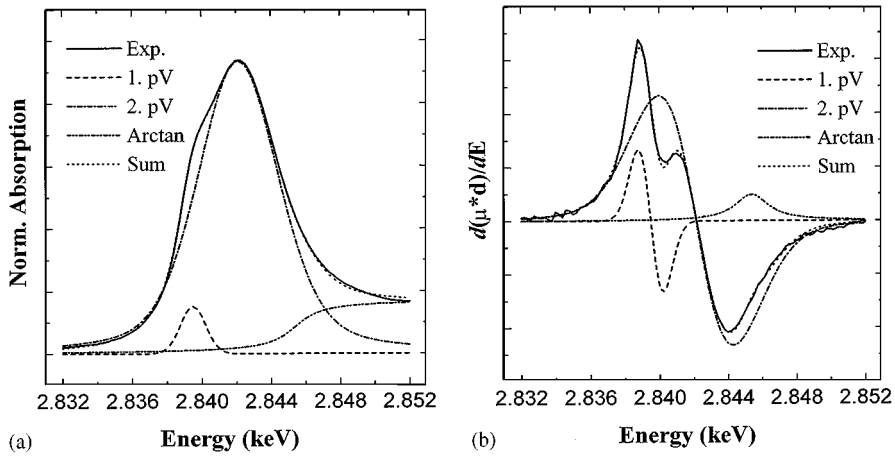

FIG. 5. (a) Fit of the Ru–L_{III} XANES of $Sr_2Cu_{0.1}Ru_{0.9}O_4$ (pV, pseudo-Voigt function; Arctan, arctangent function). (b) Same fit as in (a) but plotted for the first derivative of the data. The enhanced resolution is evident.

oxygen deficiency δ can be approximated by

$$\begin{aligned} \delta &\approx 0 \qquad\qquad \text{for } x \le 2y + 0.4 \\ \delta &\approx \frac{x}{2} - y - 0.2 \qquad \text{for } x > 2y + 0.4. \end{aligned} \tag{1}$$

As mentioned above, the Cu–L_{III} XANES data indicate that the oxidation state of copper remains $2+$ in all samples. Therefore, for ratios $x > 2y$ and $\delta = 0$, charge balance can be achieved only by a partial oxidation of Ru^{4+} to Ru^{5+} (or even higher oxidized species like Ru^{6+}).

Equation [1] leads to the following expression for the average oxidation number n of the ruthenium ions:

$$\begin{aligned} n &= \frac{x}{y} + 2 \qquad \text{for} \quad x \le 2y + 0.4 \\ n &= \frac{0.4}{y} + 4 \quad \text{for} \quad x > 2y + 0.4. \end{aligned} \tag{2}$$

Figure 4 shows that the white lines follow exactly the expected behavior: With increasing values of n, higher energy positions and more pronounced splittings of the lines are observed.

For a quantitative analysis, the Ru–L_{III} XANES data between 2.832 and 2.852 keV were fitted by a least-squares algorithm. Because of their better resolution the first derivatives of the spectra were used. Figures 5a and 5b show as an example the results for the compound $Sr_2Cu_{0.1}Ru_{0.9}O_4$. While in the original data the first white line is barely visible as a small shoulder, its contribution is by far more pronounced when the first derivative of the spectrum is calculated.

To describe the Ru–L_{III} XANES two pseudo-Voigt functions and one arctangent function were used. While the two pseudo-Voigt functions modeled the transitions $2p \rightarrow 4d(t_{2g})$ and $2p \rightarrow 4d(e_g)$, respectively, the arctangent was assigned to the absorption edge jump. In order to achieve stable fit results two restrictions had to be applied to the latter function: First its full width at half maximum (FWHM) was fixed to a value of 3 eV, estimated from the data given in (18). Second its energy position was restrained to be higher than the one of the second white line. The physical meaning of this restriction is the fact that the d orbitals possess lower energies than the absorption edge, which reflects a transition to the continuum.

The fit results are summarized in Table 1. We do not list the estimated standard derivations (esd) calculated by the fitting program because we believe they were unreliably small (in the order of 10^{-10} and 10^{-9} keV for energy positions and FWHMs, respectively, and 10^{-6} for the peak heights and Gaussian contributions). From our experience (i.e., from repeating the fits several times) we assume that the errors are in the order of the last digits given in Table 1.

The fit parameters can be separated into three categories: (i) A linear increasing between $4 \le n \le 5$ and constant values for $n > 5$ were observed for the energy shift, height and intensity of the first white line and for the energy shift of the second white line. (ii) The values of the Gaussian contributions η of both pseudo-Voigt functions and of the FWHM of the second pseudo-Voigt function decreased linearly with increasing n and remained constant for $n > 5$. (iii) Basically constant values were found for the position, height, and integrated intensity of the arctangent function and for the height, and intensity of the second pseudo-Voigt function. Only the FWHM of the first peaks does not belong to any of these categories as will be discussed below.

As the two pseudo-Voigt functions can be assigned to transitions of a $2p$ electron to unoccupied t_{2g} and e_g electronic states, respectively, their positions and intensities yield valuable information about the corresponding orbitals: As shown in Fig. 6 the energy positions of both the

TABLE 1
Results of the XANES-Fits at the Ru–L_{III}-threshold[a]

Sample	n		E(keV)	PeakHeight (ar.un.)	FWHM (eV)	η	Integrated Intensity (ar.un.)
Sr_2RuO_4	4.000	pV1	2.83932	0.661	1.86	0.89	1.17E-3
		pV2	2.84186	4.564	6.32	0.66	2.94E-2
		arctan	2.84500	0.863			5.88E-3
RuO_2*	4.000	pV1	2.83928	0.770	1.82	0.96	1.28E-3
		pV2	2.84190	4.712	6.00	0.55	3.00E-2
		arctan	2.84505	0.676			3.54E-3
$x = 1.86$, $y = 0.9$	4.067	pV1	2.83938	0.753	1.94	0.83	1.44E-3
		pV2	2.84201	4.480	6.32	0.71	2.78E-2
		arctan	2.84511	0.830			8.30E-1
$x = 2.0$, $y = 0.9$	4.222	pV1	2.83948	0.780	2.02	1.00	1.39E-3
		pV2	2.84212	4.716	6.38	0.68	3.00E-2
		arctan	2.84539	0.803			4.65E-3
$x = 1.58$, $y = 0.7$	4.257	pV1	2.83943	1.044	2.22	0.62	2.56E-3
		pV2	2.84232	4.254	6.14	0.56	2.75E-2
		arctan	2.84584	0.759			4.40E-3
$x = 0.92$, $y = 0.4$	4.300	pV1	2.83939	1.290	2.34	1.00	2.68E-3
		pV2	2.84236	5.021	5.42	0.28	3.23E-2
		arctan	2.84613	0.650			3.98E-3
$x = 1.2$, $y = 0.5$	4.400	pV1	2.83949	1.789	2.36	0.80	4.24E-3
		pV2	2.84245	6.508	5.46	0.38	4.06E-2
		arctan	2.84580	0.936			6.05E-3
$x = 2.0$, $y = 0.8$*	4.500	pV1	2.83981	1.692	2.83	0.65	5.20E-3
		pV2	2.84269	4.755	5.58	0.47	2.94E-2
		arctan	2.84548	0.786			5.52E-3
$x = 1.76$, $y = 0.7$	4.514	pV1	2.83976	1.797	2.82	0.73	5.23E-3
		pV2	2.84272	4.998	5.50	0.42	3.10E-2
		arctan	2.84579	0.791			4.75E-3
$x = 1.30$, $y = 0.5$	4.600	pV1	2.83994	1.940	2.96	0.61	6.27E-3
		pV2	2.84298	4.414	4.90	0.38	2.49E-2
		arctan	2.84566	0.735			4.60E-3
$Ba_5Ru_3O_{12}$*	4.670	pV1	2.83998	1.823	3.24	0.41	7.03E-3
		pV2	2.84307	3.534	4.64	0.19	2.04E-2
		arctan	2.84581	0.733			3.70E-3
$x = 1.40$, $y = 0.5$	4.800	pV1	2.84017	3.154	2.76	0.26	1.10E-2
		pV2	2.84325	5.369	4.20	0.31	2.64E-2
		arctan	2.84533	1.025			4.64E-3
$x = 1.70$, $y = 0.5$*	4.800	pV1	2.84037	3.068	2.35	0.16	9.90E-3
		pV2	2.84342	5.136	3.80	0.14	2.51E-2
		arctan	2.84500	0.904			5.16E-3
$x = 1.16$, $y = 0.4$	4.900	pV1	2.84023	2.753	2.60	0.12	9.76E-3
		pV2	2.84329	4.557	3.98	0.29	2.23E-2
		arctan	2.84532	0.872			6.08E-3
$x = 1.52$, $y = 0.4$	5.000	pV1	2.84060	3.830	2.24	0.25	1.12E-2
		pV2	2.84359	6.695	3.46	0.04	3.17E-2
		arctan	2.84426	0.995			7.87E-3
$Sr_4Ru_2O_9$*	5.000	pV1	2.84045	2.701	2.74	0.03	9.68E-3
		pV2	2.84352	3.415	3.98	0.42	1.58E-2
		arctan	2.84541	0.882			5.17E-3
$Ba_5Ru_2O_9(O_2)$*	5.000	pV1	2.84043	2.954	2.52	0.08	1.03E-2
		pV2	2.84354	4.496	3.67	0.27	2.05E-2
		arctan	2.84525	0.954			6.04E-3
$x = 1.44$, $y = 0.3$*	5.333	pV1	2.84057	4.237	2.24	0.28	1.21E-2
		pV2	2.84350	7.867	3.45	0.15	3.55E-2
		arctan	2.84520	0.995			6.75E-3
$x = 1.16$, $y = 0.3$	5.333	pV1	2.84045	3.640	2.12	0.41	9.31E-3
		pV2	2.84340	6.782	3.56	0.02	3.25E-2
		arctan	2.84598	0.832			3.80E-3

[a] n, Average Ru oxidation number according to Eq. [2]; η, Gaussian contribution to the pseudo-Voigt functions; pV1, pV2, first and second pseudo-Voigt function; arctan, arctangent function; *, Average of two measurements.

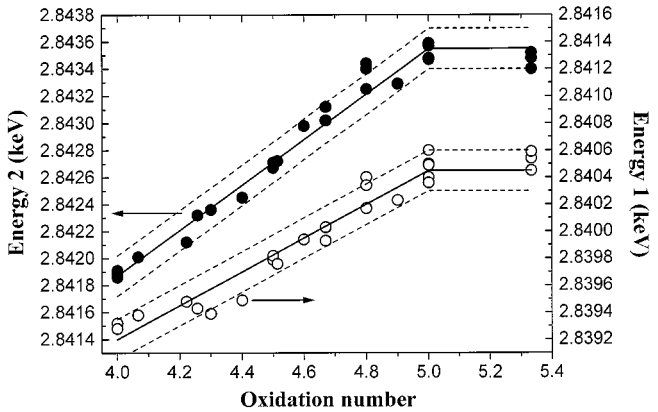

FIG. 6. Energy position of the t_{2g} (right scale, open symbols)- and e_g-related white lines (left scale, filled symbols) as a function of the calculated oxidation number n. Solid lines represent the result of a linear regression, dashed lines represent a $\pm$ 0.15-eV interval.

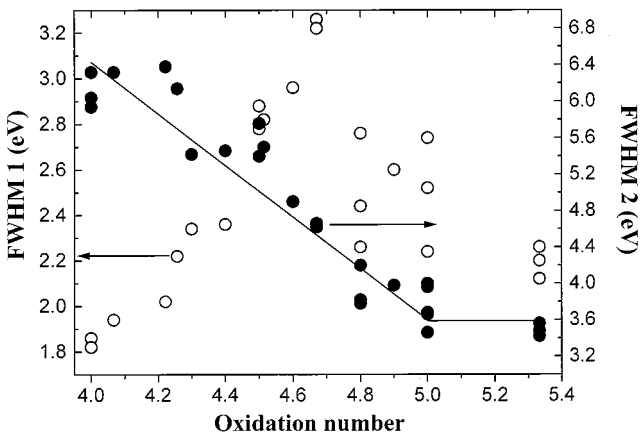

FIG. 7. Influence of the Ru oxidation state on the full width at half maximum (FWHM) of the first (left scale, open symbols) and second pseudo-Voigt function (right scale, filled symbols). Lines are just to guide the eye.

first and the second white line are shifted to higher energies with increasing n as predicted by the valence shift effect. It is noteworthy that the values for the reference materials with Ru^{4+}, $Ru^{4.67+}$, and Ru^{5+} lie exactly on the same line as for all samples of the system $La_{2-x}Sr_xCu_{1-y}Ru_yO_{4-\delta}$. For $n \geq 5$ the positions of both white lines are the same as for the Ru^{5+} standards. We therefore conclude that in $La_{2-x}Sr_xCu_{1-y}Ru_yO_{4-\delta}$ ruthenium is progressively oxidized from 4 + to 5 + while no Ru^{6+} is formed.

The energy positions of the white lines showed the least scattering of all parameters. We therefore have fitted these data with a linear regression between $4 \leq n \leq 5$, yielding

$$E[\text{keV}] = 2.83420 + 1.25 \times 10^{-3} \cdot n \qquad [3]$$

for the first white line and

$$E[\text{keV}] = 2.83515 + 1.68 \times 10^{-3} \cdot n \qquad [4]$$

for the second white line, respectively.

As can be seen from Fig. 6 almost all data points lie within a band of $\pm$ 0.15 eV around the calculated values. Compared to the total energy difference of ca. 1.7 eV between the Ru^{4+} and Ru^{5+} compounds this means a deviation of less than 10%. Therefore, the energies of the white lines are an excellent measure for the oxidation state of ruthenium.

Figure 6 also shows that the values for the first peak scatter slightly more than those for the second one. This is not surprising as the intensity of the first white line is rather small (see Fig. 5) and therefore the fit results are expected to exhibit larger uncertainties. For this reason we conclude that the position of the second white line is the most reliable parameter for the determination of the Ru valence.

As the energy position of the second pseudo-Voigt function increases, its full width at half maximum and its Gaussian contribution η decrease (Figs. 7 and 8). Thus the peak becomes sharper and changes from a Gaussian- to a Lorenztian-type shape. A similar decrease of η was also observed for the first white line. On the other hand, an interesting exception to this behavior was found for its FWHM: Here, a maximum was observed for $n \approx 4.7$ while both higher and lower values of n led to smaller peak widths (Fig. 7).

The changes in the peak widths and shapes are not easy to explain. It has been suggested that a higher covalency of the metal–oxygen bond would lead to a broadening of the white lines. This argument has been used to explain the larger FWHM of the e_g related peak (which reflects the transition to an antibonding orbital that involves a strong covalent admixture of the ligand p-orbitals) with respect to the t_{2g}-related peak (which corresponds to a nonbonding, metal d-type orbital) (1, 19). On the other hand, the covalency of

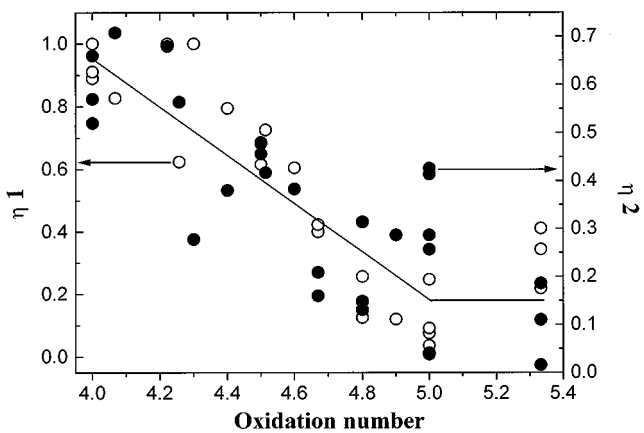

FIG. 8. Influence of the Ru oxidation state on the Gaussian contribution (η) to the first (left scale, open symbols) and second pseudo-Voigt function (right scale, filled symbols). Lines are just to guide the eye.

the Ru–O bond increases with increasing ruthenium oxidation state (20). Therefore, one would expect the white lines to be broader for Ru^{5+} than for Ru^{4+}, in contrast to what is actually found.

We assume that the observed changes in peak width and shape are due to changes in the local Ru–O geometry. As was found by XRD Rietveld refinements, the RuO_6 units in the system $La_{2-x}Sr_xCu_{1-y}Ru_yO_{4-\delta}$ are not ideal octahedra but show a slight tetragonal elongation Ref. (5). Thus, the local symmetry around the Ru ions is D_{4h} rather than O_h, and the e_g and t_{2g} orbitals split into sets of b_{1g} ($d_x^2 - d_y^2$), a_{1g} (d_z^2), and b_{2g} (d_{xy}), e_g (d_{xz}, d_{yz}), respectively. As this splitting is too small to be experimentally resolved, only the superposition of the different transitions is observed. It can easily be demonstrated that the envelope of two or more overlapping Lorentzian peaks mimics a broader, more Gaussian-shaped peak. Therefore, both the sharpening of the white lines and its change in peak shape can well be explained by a decreased tetragonal elongation of the $Ru^{5+}O_6$ unit with respect to the $Ru^{4+}O_6$ unit. An explanation for this behavior can be found by looking at the electronic configurations: Ru^{4+} with its $^3T_{1g}$ ground state is Jahn–Teller active and therefore favors a tetragonal environment while Ru^{5+} ($^4A_{2g}$) shows no Jahn–Teller effect.

Our Rietveld refinements for the system $La_{2-x}Sr_xCu_{1-y}Ru_yO_{4-\delta}$ confirm the above considerations: As these refinements only lead to an average Ru–O/Cu–O distance it is difficult to compare compounds with different Ru contents. Nevertheless, we found that in each series with constant y value the degree of elongation decreases with increasing Sr content, that is with increasing oxidation state of the ruthenium ions (5).

Although the Jahn–Teller distortion is well suited to explaining the changes in the shape and width of the second white line as well as the change in the shape of the first white line it unfortunately does not provide an explanation for the observed maximum at $n \approx 4.7$ of the FWHM of the first white line.

While the energy shift of the two white lines is due to the increasing effective core charge and hence the formation of Ru^{5+}, their energy difference (ΔE) reflects the strength of the octahedral crystal field 10Dq. It is well known that higher oxidized ions exhibit larger values of 10Dq. Looking at Fig. 9 it can be seen that ΔE follows the expected behavior, i.e., its values increase between $n = 4$ and 5. The slight decrease for the samples with $n = 5.333$ can be explained by the formation of electron holes in the oxygen $2p$ band. As these reduce the charge of the ligands, 10Dq is supposed to become smaller. On the other hand, the error bars shown in the figure indicate that the decrease is barely significant.

For Ru^{3+} ions ΔE and 10Dq are correlated by

$$10Dq = \Delta E + \xi_d \qquad [5]$$

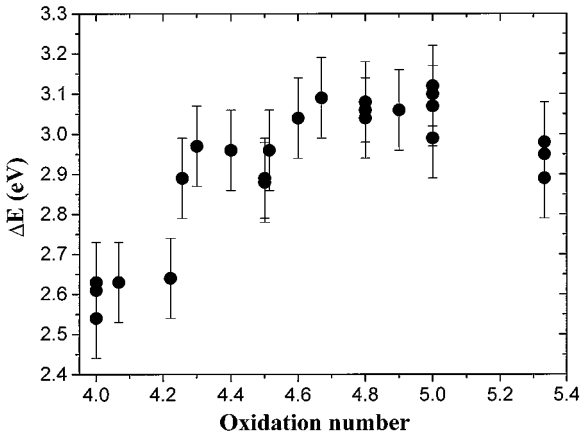

FIG. 9. Increasing splitting of the t_{2g}- and e_g-related white lines with increasing oxidation number. Error bars represent $\sqrt{2} \times 0.15$ eV.

if further splitting by a tetragonal crystal field is neglected (17) (ζ_d is the spin-orbit coupling constant). For Ru^{4+} the situation is slightly more complicated as the spin-orbit interaction splits the $^3T_{1g}$ term of the $(t_{2g}^4)(e_g^0)$ configuration into three states lying at $-2\zeta_d$, $-\zeta_d$, and $+\zeta_d$, respectively. For Ru^{5+} $(t_{2g}^3)(e_g^0)$, on the other hand, the $^4A_{2g}$ term is not split by spin orbit coupling. Nevertheless, as ζ_d is only about 0.13 eV (21), hence small compared to ΔE (2.54–3.12 eV) and of the same magnitude as the experimental error one might as well set ΔE equal to 10Dq.

In a first approximation the intensities of the two white lines should be directly proportional to the number of electron holes in the t_{2g} and e_g orbitals. Therefore, the intensity of the first peak is supposed to increase upon oxidation of the ruthenium ions while the second peak should possess a constant intensity, as for both Ru^{4+} and Ru^{5+} the e_g orbitals are completely empty. As depicted in Figs. 10 and 11 this behavior is actually found: The peak heights and intensities of the first pseudo-Voigt function increase linearly with n reflecting nicely the successive formation of vacancies in the t_{2g}-type orbitals and therefore the increasing oxidation state of the ruthenium ions. For $n \geq 5$ constant values are found, again proving that no Ru^{6+} is formed.

Figure 11 shows that the intensities of the second white lines remain basically constant for all compounds, but the values scatter strongly. One possible reason for this is the partial overlap of the second pseudo-Voigt and the arctangent function as shown in Fig. 5, which leads to uncertainties in the fit results. On the other hand, the scattering of the intensities could also be due to uncertainties in the normalization step. As stated under Experimental, this normalization was done by setting the average absorption coefficient in an interval just behind the edge jump to 1. As the second white line is much more intense than the edge jump itself, even small differences in the edge heights lead to large errors

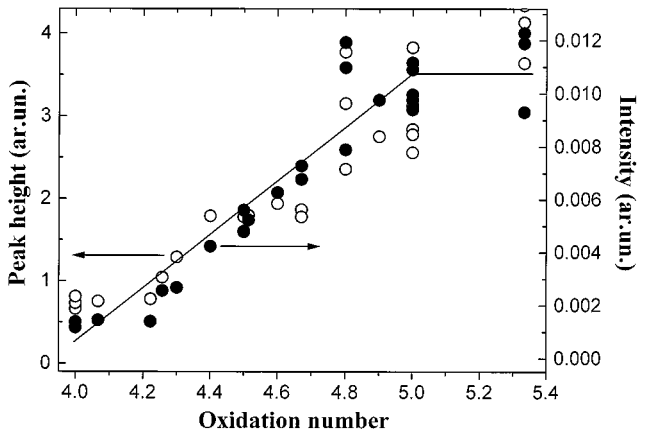

FIG. 10. The increasing peak height (left scale, open symbols) and intensity (right scale, filled symbols) of the first white line with n reflects the successive formation of holes in the t_{2g} orbitals. Lines are to guide the eye only.

for the second white line. The fact that the height (and as the FWHM was fixed also the integrated intensity) of the arctangent function also exhibits some scattering is consistent with both possible explanations.

Counting the electron holes in the t_{2g} and e_g orbitals, one would expect an intensity ratio of 2:4 for Ru^{4+} and 3:4 for Ru^{5+}, respectively. The values we actually observed are not even near to these expected ratios: For the peak heights the values range from 0.1 for $n = 4$ to 0.65 for $n = 5$, while for the integrated intensities they are even smaller (0.05 and 0.5 for $n = 4$ and 5, respectively). In a recent paper we have already analyzed the relative intensities of the white lines at the L_{III} and L_{II} thresholds of some Ru^{4+} and Ru^{5+} compounds by crystal field multiplet calculations (CFMC) (20). It turned out that for an accurate description of the peak intensities one has to take into account both the spin-orbit coupling and the interelectronic repulsion. The latter can be

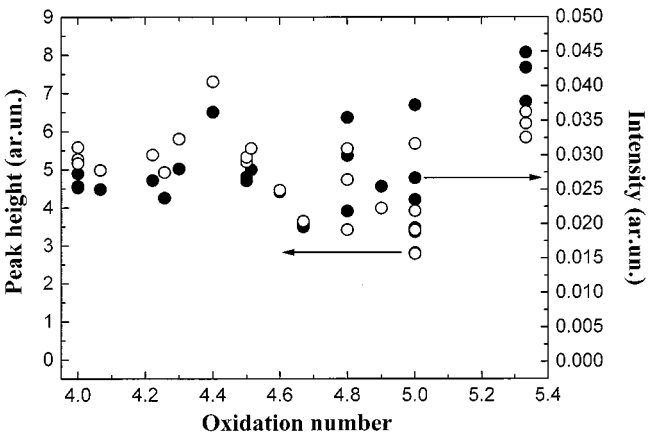

FIG. 11. Peak height (left scale, open symbols) and intensity (right scale, filled symbols) of the second white line.

described in terms of Slater integrals. The main effect of the interelectronic repulsion is a suppression of the t_{2g}- related peak at the L_{III} edge both for a d^4 and d^3 configuration. Due to the hybridization of the Ru–*d* and O–*p* orbitals the Coulomb repulsion is reduced, known as nephelauxetic effect. This effect can be taken into account by reducing the Slater integrals from their atomic values. We achieved the best agreement between experimental data and calculation by reducing the Slater integrals to 40 and 15% for Ru^{4+} and Ru^{5+}, respectively. Thus the t_{2g}-related peak is much more suppressed for Ru^{4+} than for Ru^{5+}. The t_{2g}/e_g intensity ratios observed in the system $La_{2-x}Sr_xCu_{1-y}Ru_yO_{4-\delta}$ are in good agreement with these calculations and therefore strongly support our previous results.

Very recently, Choy *et al.* have reported Ru–L_{III} XANES investigations of La_2MRuO_6 (M = Zn, Mg, and Li) and Ba_2YRuO_6, in which ruthenium takes the oxidation states 4+ and 5+, respectively (4). By fitting the second derivatives of the spectra with two Lorentzian functions, the authors got results very similar to ours: Going from Ru^{4+} to Ru^{5+} both the t_{2g}- and the e_g-related peaks were found to shift to higher energies by 1.16 and 1.40 eV, respectively. Futhermore, the height and area of the t_{2g}-related white line increased while almost constant values were found for the e_g-related peak. Although our values for the valence shifts are slightly higher (1.25 and 1.68 eV, respectively), we feel that the data given by Choy *et al.* provides an excellent confirmation of the results reported in this paper.

CONCLUSIONS

XANES spectroscopy proved to be a powerful tool to investigate the oxidation states of ruthenium and copper in the mixed valence system $La_{2-x}Sr_xCu_{1-y}Ru_yO_{4-\delta}$.

By comparing the XANES features with well characterized reference compounds we found that at the Cu–L_{III} threshold almost all samples exhibited the same structure as the Cu^{2+} standard CuO. We therefore conclude that copper possesses the oxidation state 2+ in all samples. Only for very high ratios of $x/2y$ did a shoulder appear, indicating the formation of electron holes in the 2*p* band of the oxygen ligands.

At the Ru–L_{III} threshold, on the other hand, we found a successive change from a behavior typical for Ru^{4+} compounds to one observed for the Ru^{5+} reference samples. Two white lines were observed, corresponding to the transitions $2p \rightarrow 4d(t_{2g})$ and $2p \rightarrow 4d(e_g)$. These white lines could well be fitted by two pseudo-Voigt type functions. From the approximation for the oxygen deficiency δ we derived an equation describing the average oxidation state (n) of the ruthenium ions. The great majority of the refined parameters of the pseudo-Voigt functions showed a linear dependence on n between $n = 4$ and $n = 5$ while they remained constant for $n \geq 5$. This behavior reflects the

successive oxidation of Ru^{4+} to Ru^{5+} and proves that no Ru^{6+} ions are present.

It should be stressed that the parameters of the reference compounds and the samples of the $La_{2-x}Sr_xCu_{1-y}Ru_yO_{4-\delta}$ system exhibit the same behavior; i.e., in a graphical representation their values fall on one straight line. This proves that the described XANES analysis is not restricted to one specific system but can be applied to a large variety of ruthenates. As long as ruthenium is in a sixfold oxygen coordination, it does not matter how these RuO_6 units are connected: They can be face sharing (like in $Sr_4Ru_2O_9$, $Ba_5Ru_2O_9(O_2)$, and $Ba_5Ru_3O_{12}$), edge sharing (RuO_2), or corner sharing ($La_{2-x}Sr_xCu_{1-y}Ru_yO_{4-\delta}$). Neither does the nature of the A-type cations (Ba, Sr, La) or even their absence (RuO_2) have any influence on the spectra.

Among the refined parameters the intensity of the first white line and the energy positions of the first and second white lines are the most relevant: The former reflects directly the formation of electron holes in the t_{2g} orbitals while the latter two are affected by the valences shift effect; i.e., their values increase with increasing oxidation state. The energy difference between the t_{2g}- and e_g-related peaks at the Ru–L_{III} threshold was found to increase with n, which is in agreement with the general trend of the octahedral crystal field splitting 10Dq to become larger with increasing oxidation state.

The energy shift of the second white line showed the least scattering of all parameters and is therefore best suited for a quantitative analysis. A linear regression was applied for $4 \leq n \leq 5$, yielding $E[\text{keV}] = 2.83515 + 1.68 \times 10^{-3} \cdot n$. This linear relationship allows one to determine the oxidation state of Ru in unknown compounds (i.e., to derive n from an experimentally found value of E). As the deviation of the data points from the calculated values was ≤ 0.15 eV for almost all compounds under investigation, we conclude that an accuracy of $\pm 10\%$ can be achieved. This means that one should be able to distinguish Ru ions with an average oxidation state of, say, 4.4+ and 4.6+, respectively. It is noteworthy that the determination of ruthenium oxidation states via XANES is quite simple: Basically, only three measurements (for a Ru^{4+} and a Ru^{5+} reference and for the sample itself) have to be carried out to derive the valence within a reasonable accuracy.

Because it is element-specific, XANES spectroscopy is especially interesting for those oxides, which contain more than one mixed-valence element. The only requirement these compounds must meet is that they contain Ru in an (octahedral) oxygen coordination sphere. Otherwise, the valence shift might be modified by the chemical shift.

Finally we emphasize that the linear relationship between the energy shift and the calculated average oxidation state is an excellent confirmation for the thermogravimetrically derived formula of the oxygen deficiency δ. It should be noted that this formula was originally intended to be just a rough *approximation* for the influence of x and y on δ. Keeping this in mind the little scattering of the data points is rather astonishing.

ACKNOWLEDGMENTS

The authors thank Prof. Jacques Darriet and Dr. Fabien Grasset at ICMCB, Bordeaux, for kindly providing samples of $Ba_5Ru_2O_9(O_2)$, $Sr_4Ru_2O_9$, and $Ba_5Ru_3O_{12}$. Furthermore, we thank the HASYLAB for allocating beamtime. This work was supported by the Deutsche Forschungsgemeinschaft (SFB 484).

REFERENCES

1. J. H. Choy, D. K. Kim, G. Demazeau, and D. Y. Jung, *J. Phys. Chem.* **98,** 6258 (1994).
2. J. H. Choy, D. K. Kim, S. H. Hwang, G. Demazeau, and D. Y. Jung, *J. Am. Chem. Soc.* **117,** 8557 (1995).
3. J. H. Choy, D. K. Kim, and J. Y. Kim, *Solid State Ionics* **108,** 159 (1998).
4. J. H. Choy, J. Y. Kim, S. H. Hwang, S. J. Kim, and G. Demazeau, *Int. J. Inorg. Mater.* **2,** 61 (2000).
5. S. Ebbinghaus and A. Reller, *Solid State Ionics* **101–103,** 1369 (1997).
6. S. Ebbinghaus, M. Fröba, and A. Reller, *J. Phys. Chem. B* **101,** 9909 (1997).
7. F. Grasset, C. Dussarrat, and J. Darriet, *J. Mater. Chem.* **7,** 1911 (1997).
8. C. Dussarrat, J. Fompeyrine, and J. Darriet, *Eur. J. Solid State Chem.* **32,** 3 (1995).
9. C. Dussarrat, F. Grasset, R. Bondtchev, and J. Darriet, *J. of Alloys Compd.* **233,** 15 (1996).
10. T. Ressler, *J. Phys. IV* (*France*) **7,** C2–C269 (1997).
11. Z. Hu, C. Mazumdar, G. Kaindl, F. M. F. de Groot, S. A. Warda, and D. Reinen, *Chem. Phys. Lett.* **297,** 321 (1998).
12. P. V. Avramov, S. G. Ovchinnikov, V. A. Gavrichkov, and S. Ph Ruzankin, *Physica C* **278,** 94 (1997).
13. G. Kaindl, O. Strebel, A. Kolodziejczyk, W. Schäfer, R. Kiemel, S. Lösch, S. Kemmler-Sack, R. Hoppe, H. P. Müller, and D. Kissel, *Physica B* **158,** 446 (1989).
14. O. Strebel, G. Kaindl, A. Kolodziejczyk, W. Schäfer, R. Kiemel, S. Lösch, and S. Kemmler-Sack, *J. Magn. Magn. Mater.* **76** and **77,** 97 (1988).
15. Y. Seino, K. Okada, and A. Kotani, *J. Phys. Soc. Jpn.* **59,** 1384 (1990).
16. S. Ebbinghaus, Ph.D. thesis, Univ. of Hamburg, 1998.
17. T. K. Sham, *J. Am. Chem. Soc.* **105,** 2269 (1983).
18. M. O. Krause and J. H. Oliver, *J. Phys. Chem. Ref. Data* **8,** 329 (1979).
19. C. Sugiura, M. Kitamura, and S. Muramatsu, *J. Chem. Phys.* **84,** 4824 (1986).
20. Z. Hu, H. von Lips, M. S. Golden, J. Fink, G. Kaindl, F. M. F. de Groot, S. Ebbinghaus, and A. Reller, *Phys. Rev. B* **61,** 5262 (2000).
21. J. S. Griffith, "The Theory of Transistion-Metal Ions: Cambridge Univ. Press," New York, 1961.